remote sensing

MDPI

Article

Precise Positioning of BDS, BDS/GPS: Implications for Tsunami Early Warning in South China Sea

Kejie Chen *, Natalia Zamora, Andrey Y. Babeyko, Xingxing Li and Maorong Ge

Received: 30 September 2015; Accepted: 23 November 2015; Published: 30 November 2015
Academic Editors: Zhenhong Li, Roberto Tomas, Xiaofeng Li and Prasad S. Thenkabail

GFZ German Research Centre for Geoscience, Telegrafenberg, 14473 Potsdam, Germany; zamora@gfz-potsdam.de (N.Z.); babeyko@gfz-potsdam.de (A.Y.B.); lixin@gfz-potsdam.de (X.L.); maor@gfz-potsdam.de (M.G.)
* Correspondence: kejie@gfz-potsdam.de; Tel.: +49-331-2882-8792

Abstract: Global Positioning System (GPS) has been proved to be a powerful tool for measuring co-seismic ground displacements with an application to seismic source inversion. Whereas most of the tsunamis are triggered by large earthquakes, GPS can contribute to the tsunami early warning system (TEWS) by helping to obtain tsunami source parameters in near real-time. Toward the end of 2012, the second phase of the BeiDou Navigation Satellite System (BDS) constellation was accomplished, and BDS has been providing regional positioning service since then. Numerical results indicate that precision of BDS nowadays is equivalent to that of the GPS. Compared with a single Global Satellite Navigation System (GNSS), combined BDS/GPS real-time processing can improve accuracy and especially reliability of retrieved co-seismic displacements. In the present study, we investigate the potential of BDS to serve for the early warning system of tsunamis in the South China Sea region. To facilitate early warnings of tsunamis and forecasting capabilities in this region, we propose to distribute an array of BDS-stations along the Luzon Island (Philippines). By simulating an earthquake with Mw = 8 at the Manila trench as an example, we demonstrate that such an array will be able to detect earthquake parameters in real time with a high degree of accuracy and, hence, contribute to the fast and reliable tsunami early warning system in this region.

Keywords: BDS; BDS/GPS; South China Sea; tsunami early warning system

1. Introduction

As one of the most devastating natural coastal disasters, tsunamis are triggered mostly by shallow earthquakes in submarine subduction zones [1] producing the most damage in the near field but also propagating basin-wide. Consequently, traditional Tsunami Early Warning Systems (TEWS) mainly rely on seismic methods in order to evaluate source parameters (magnitude, epicenter) and forecast tsunamis as soon as possible. Corresponding seismic instrumentation mainly includes broadband seismometers as well as strong-motion sensors (accelerometers). Despite the fact that these traditional techniques have proved their reliability for most historical cases over the last decades, they have failed to provide correct rapid magnitude estimation for several important events like the 2004 Mw = 9.3 Great Sumatra earthquake, the 2010 Mw = 7.8 Mentawai tsunami earthquake and the 2011 Mw = 9.0 Great Tohoku event. For example, in the latter case, the true magnitude was significantly underestimated during the fifty minutes after the earthquake [2]. Magnitude underestimation, in turn, may result in the underestimation of the tsunami forecast in the near field [2].

The reasons for magnitude underestimation during the first several minutes after large earthquakes vary for different seismic instruments as well as earthquake evaluation procedures.

Broadband seismometers saturate near the source in case of strong shaking so that the full rupture image can be analyzed only at larger epicentral distances, causing unavoidable delay due to the finite speed of seismic wave propagation. Strong motion sensors, in turn, do not saturate by amplitude and can be employed close to the source; however, the usual band-pass filtering of waveforms aimed to avoid processing unambiguity caused by co-seismic tilting [3] effectively leads to magnitude saturation due to removal of long periods which are essential for huge earthquakes [4]. See, for example, [2,5] regarding the analysis of the strong-motion magnitude saturation during the Great Tohoku earthquake.

The 2004 Great Mw = 9.3 Sumatra earthquake and tsunami boosted the development of new seismic approaches that are aimed toward the faster and more reliable characterization of tsunamigenic earthquakes. During the GITEWS Project (German-Indonesian Tsunami Early Warning System), Bormann and Saul [6] proposed a fast, non-saturating cumulative magnitude estimator based on the P-wave train. The procedure was tested at epicentral distances starting from 5° and is currently operated by the INATEWS (Indonesian Tsunami Early Warning System) [7]. Additionally, Kanamori and Rivera [8] suggested a new broadband W-phase source inversion algorithm, which is currently running in operation at PTWC (Pacific Tsunami Warning Center). During the 2011 Great Mw = 9.0 Tohoku event, this algorithm automatically detected the focal mechanism and came with magnitude estimate of Mw = 8.8 22 min after the earthquake (the true magnitude Mw = 9.0 was estimated 40 min after the earthquake) [9]. Another approach was suggested by Lomax and Michelini [10], who introduced an original duration-amplitude procedure to estimate the tsunamigenic potential of earthquakes.

Significant efforts were also undertaken to improve the quality of real-time strong-motion data processing. New studies [4,11,12] proposed fast and effective procedures for automatic base-line correction. Furthermore, the novel technique of collocation of strong-motion and GPS sensors [13,14] should help to overcome the problem of magnitude saturation since the band-pass filtering is no longer required [15].

Rapid improvement of the real-time GPS processing precision put GPS-technology at the front end of current progress in the earthquake and tsunami early warning system. Compared with seismic approaches, continuous GNSS real-time data processing provides arbitrary ground displacements that can be directly inverted into source parameters in (near-) real time. Hence, it is considered to be a more trustworthy tool, especially for the near field tsunami early warning. Several previous studies have discussed or demonstrated the potential of using GPS data for tsunami early warnings. For example, Blewitt *et al.* [16] showed that the magnitude, mechanism, and spatial extent of rupturing of the 26 December 2004 Sumatra earthquake might have been accurately determined using only 15 min of GPS data following an earthquake initiation. Simultaneously, Sobolev *et al.* [17] pointed out that the reliable prediction of tsunami waves on the Indonesian coast can be issued within less than 5 min of an earthquake by incorporating special types of near-field GPS arrays ("GPS-Shield" concept for Indonesia). They also proposed deployment of such arrays for other tsunamigenic active regions. Following this idea, GITEWS (German Indonesian Tsunami Early Warning System) became the first TEWS to implement real-time GPS for a tsunami early warning [18,19]. Recently, Hoechner *et al.* [20] replayed the Great Tohoku 2011 event in that they presented a complete processing chain starting from actual raw GPS data and fully simulated the situation as it would be in a warning center ending up with a very fast and qualified tsunami early warning. Now using real-time GPS for earthquake and tsunami early warnings is an active area of research (e.g., [18–26]).

To date, geo-hazard monitoring with GNSS is restricted to the oldest, largest and most-used GPS system. Around the end of 2012, China has completed the regional constellation of the BeiDou Satellite System (BDS), and the system has been running routinely since then. Even at its second-phase stage, numerous studies (e.g., [27–29]) have demonstrated that precise positioning performance of BDS is equal in match against that of GPS in the Asia-Pacific region. Compared with a single satellite navigation system, the fusion of GPS, GLONASS, GALILEO and BDS can significantly

increase the number of observed satellites, reduce the position dilution of precision (PDOP) [29] and, thus, increase robustness and the reliability of observations. What is more, BDS, due to its similarity to GPS signal structure and frequencies, provides a much better chance for investigating the impact of multi-GNSS capacity on real-time precise positioning in terms of accuracy and reliability. In the present study, we investigate the potential of the BDS system to contribute to the tsunami early warning system in the South China Sea region. In particular, we assess the accuracy of the real-time BDS processing and corresponding source inversion due to a hypothetical tsunamigenic earthquake at the Manila trench.

As shown in previous studies (e.g., [30–33]), the Manila subduction zone (Figure 1) has been identified as a zone of potential tsunami hazard in the SCS region. Despite the absence of clear historical evidence on large tsunamis generated at the Manila trench, tsunami deposits found at the Xischa Islands (~1024 AD) may be attributed to a large event in this source region [34]. According to the recently compiled historical tsunami database for the northeastern South China Sea [35], annual probability of a tsunami in this region from any source is very high (~33%). However, the likelihood of a damaging tsunami per year is much smaller (1%–2%). In the absence of large historical events from the Manila Trench, damaging tsunamis in the South China Sea have been previously studied by means of numerical modeling. Simulations [30,36] suggest that an earthquake with a magnitude of Mw = 8.0 or larger at the Manila trench may cause significant tsunami damage along the whole south-eastern coast of China, Southwestern Taiwan and West Philippines. Taking the potential large-scale disaster into account, the tsunami early warning system in the SCS region was suggested by [30,37,38] based on DART-type deep ocean buoys. In fact, China has installed two buoys in SCS in 2014. In the present paper, we propose to improve the regional TEWS by installing real-time continuous BDS-network at the Luzon Island, Philippines. Being integrated with traditional seismic networks, the proposed GNSS-array will contribute to fast and reliable source inversion, which is one of the most important tasks in the early warning and forecasting of tsunamis.

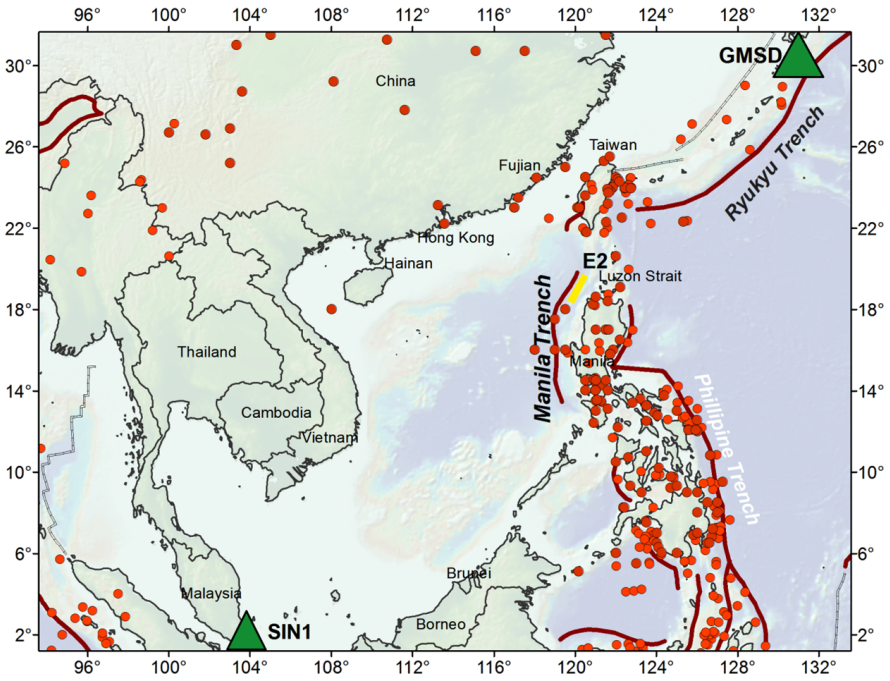

Figure 1. Seismotectonic map of the Southern China Sea. The red thick line represents the Manila trench of the seismogenic Manila subduction zone. The red points show the earthquakes that have occurred from 1976 to 2015 with a magnitude larger than Mw = 6.5 (GCMT catalog). The yellow line E2 indicates the rupture area used in this study. The two multi-GNSS stations used in Section 2 are also shown by green triangles.

In Section 2, we test the real-time precise positioning performance of BDS and compare it with GPS and joint BDS/GPS in the SCS region. In Section 3, we simulate a test scenario of an Mw = 8.0 earthquake along the Manila trench and its corresponding tsunami to demonstrate the feasibility of incorporating BDS, BDS/GPS into the regional TEWS. In Section 4, we discuss additional issues related to the performance of BDS, BDS/GPS based TEWS. Finally, Section 5 summarizes results and presents an outlook.

2. Real-Time Kinematic Precise Positioning Performance of BDS in South-East Asia

Generally, there are two kinds of precise positioning algorithms, *i.e.*, relative positioning and single-point positioning. With respect to relative positioning, most of the error budgets can be cancelled through double differencing between reference station and rover station; as a result, its mathematical model is relatively simple and easy to be conducted. Most importantly, double-differencing integer-cycle phase ambiguities can be resolved to their correct integer values, reliably ensuring its high precision. However, the reference station of relative positioning must be fixed, which requires that, during an earthquake, it should be located outside the zone of deformation. The latter cannot always be satisfied, especially during large tsunamigenic earthquakes [21]. By contrast, the single-point positioning approach does not need a fixed reference station to form double-difference observations and, in theory, is more desirable for the retrieval of co-seismic displacements [25]. Nonetheless, it should be pointed out that for Precise Point Positioning (PPP), ambiguity resolution needs a convergence phase that may be as long as 20 min. Fortunately, the Variometric Approach for Displacements Analysis Stand-alone Engine (VADASE) [39] and the Temporal Point Positioning (TPP) [40] are able to overcome this disadvantage. The TPP has been employed in this study.

Up to now, no BDS or BDS/GPS data recorded during an earthquake is publicly available. Considering that performances of GNSS positioning are not different between earthquake-free and earthquake-breaking periods [13], to exploit the potential of BDS and BDS/GPS in retrieving co-seismic displacements, we selected two weeks of data (from 29 December 2013 to 11 January 2014) from IGS Multi-GNSS Experiment (MGEX) stations in the Asia-Pacific region. In this case, data from a 1-Hz sampling rate MGEX stations GMSD and SIN1 were used (see station distribution in Figure 1). Since no earthquake happened, we take zero displacement as ground truth. In this paper, real-time precise BDS/GPS orbits and clocks were produced according to the strategies suggested by Li *et al.* [29]. For every station, the length of each TPP session was set to 10 min, and, in each individual hour, we employed four sessions with evenly distributed start points; in total, we have 96 sessions per day for two weeks, which ensures a more trustworthy conclusion on the precise positioning performance. Figure 2 presents the TPP results in modes of BDS-only, GPS-only and BDS/GPS at station GMSD which can be taken as a typical example. As clearly shown, BDS-only and GPS-only show similar positioning performances while a BDS/GPS combined solution significantly improves the accuracy. Statistical Root Mean Square (RMS) is summarized in Table 1.

Table 1. Expected RMS of BDS, GPS, and joint BDS/GPS real-time precise positioning using TPP in South-East Asia.

RMS (m)	BDS	GPS	BDS/GPS
East	0.0095	0.0071	0.0049
North	0.0068	0.0101	0.0048
Up	0.0203	0.0207	0.0098

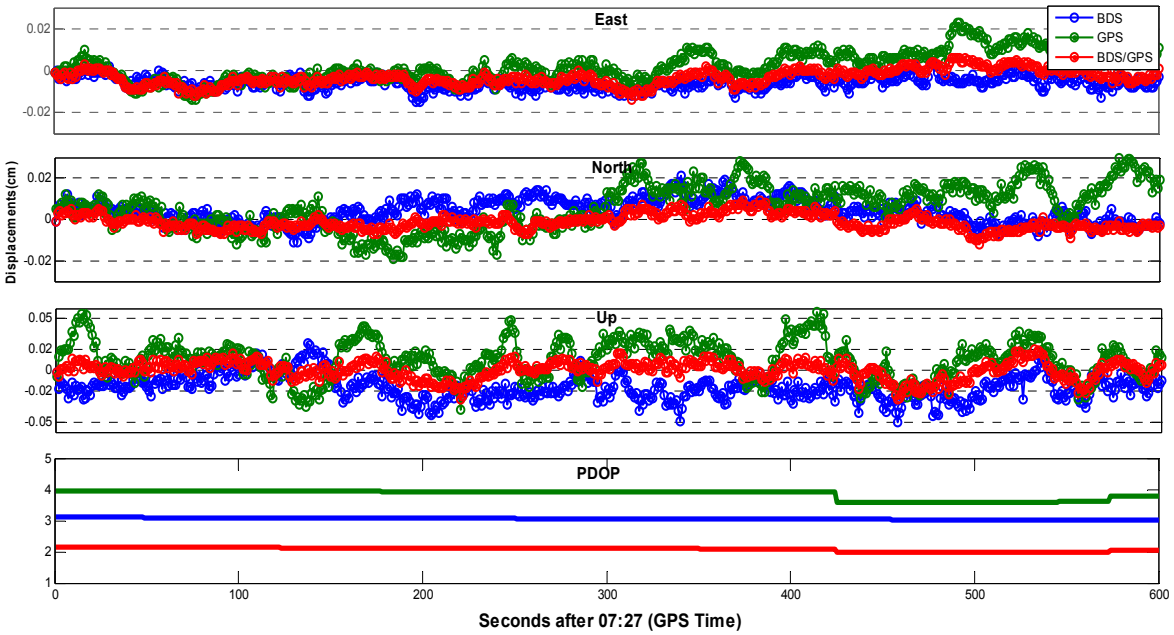

Figure 2. TPP solutions of BDS, GPS and BDS/GPS at stationary station GMSD on 30 December 2013. Additionally shown is the corresponding PDOP, which specifies the effect of navigation satellite constellation geometry on positional precision. Note that, since the station did not move, the above graphs can be used to evaluate the expected uncertainty of TPP displacements.

3. Testing the Feasibility of BDS Real-Time Network at the Luzon Island for the Tsunami Early Warning in the South China Sea

In this section, we demonstrate the feasibility of BDS for the tsunami early warning in the Southern China Sea. To do that, we simulate a hypothetical tsunamigenic earthquake along the Manila trench and try to invert resulting co-seismic displacements at a virtual BDS/GPS array distributed along the Luzon Island, northern Philippines. Previously, Kirby and Geist [41] and Liu *et al.* [30] assessed tsunamigenic potential of six rupture scenarios along the Manila trench. We follow their approach and place our fault model along the northern part of the Manila subduction zone (Figure 1). Fault parameters correspond to the rupture model E2 from Liu *et al.* (2006). This rupture scenario was selected due to its highest impact potential for the south Chinese coast. The accepted source model has a magnitude of Mw = 8.0 with the central point located at 119.8° E/18.7° N. The length is 180 km, the width 35 km, and the strike and the dip angles of the rupture plane are fixed to 35 and 20 degrees. The only difference with the original E2 rupture model is in slip distribution: we use a bell-shaped distribution rather than a uniform slip. The rupture plane consists of 75 sub-faults with a symmetry maximum at the slip center, and with the rake angles varying between 80 and 100 degrees.

We use code QSSP developed by Wang [42] to calculate synthetic displacement waveforms at stations of our virtual GNSS-array. With respect to the Earth model, in this study, the average global 1-D reference earth model AK135Q [43] is adopted. Figure 3 demonstrates simulated displacement waveforms at the selected station B1 (see virtual array in Figure 4a). To make our test even more realistic, we contaminate synthetic co-seismic displacements with a typical real-time BDS and BDS/GPS processing noises derived from a random segment of the GMSD (or SIN1) residual displacement time series, and the corresponding "noisy" displacements are also shown at Figure 3. These "noisy" displacements will be used for source inversion.

Figure 4a presents an overview of our forward rupture model: It shows assumed slip distribution together with the corresponding co-seismic vertical deformation as well as horizontal static offsets at the virtual BDS/GPS network.

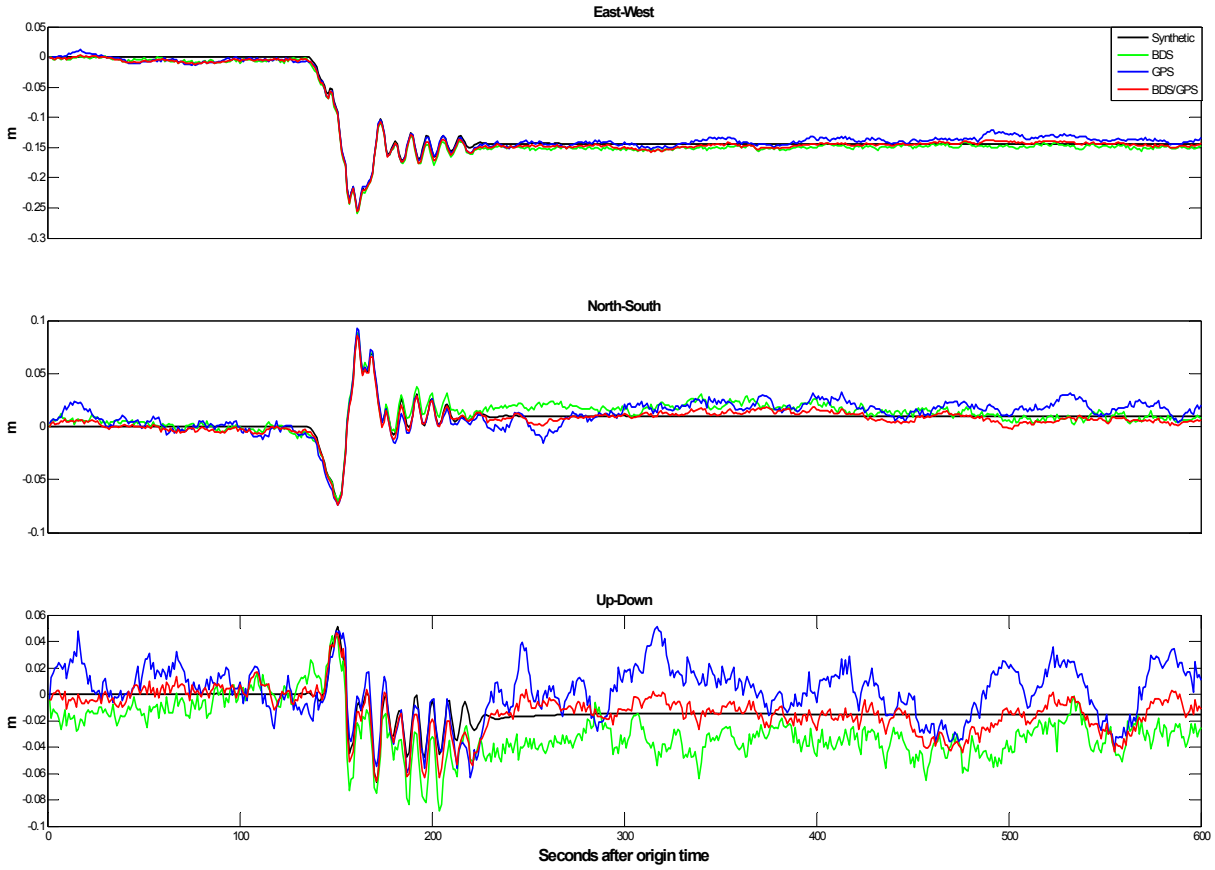

Figure 3. Simulated displacement waveforms in forward-model scenario (rupture E2, see text for description). Waveforms are shown at one selected virtual GNSS-station placed at the Luzon Island (contoured triangle on Figure 4a). Black lines represent original kinematic simulations; colored lines represent the simulations after an addition of typical TPP processing noise (Section 2). "Noisy" displacements will be used for source inversion.

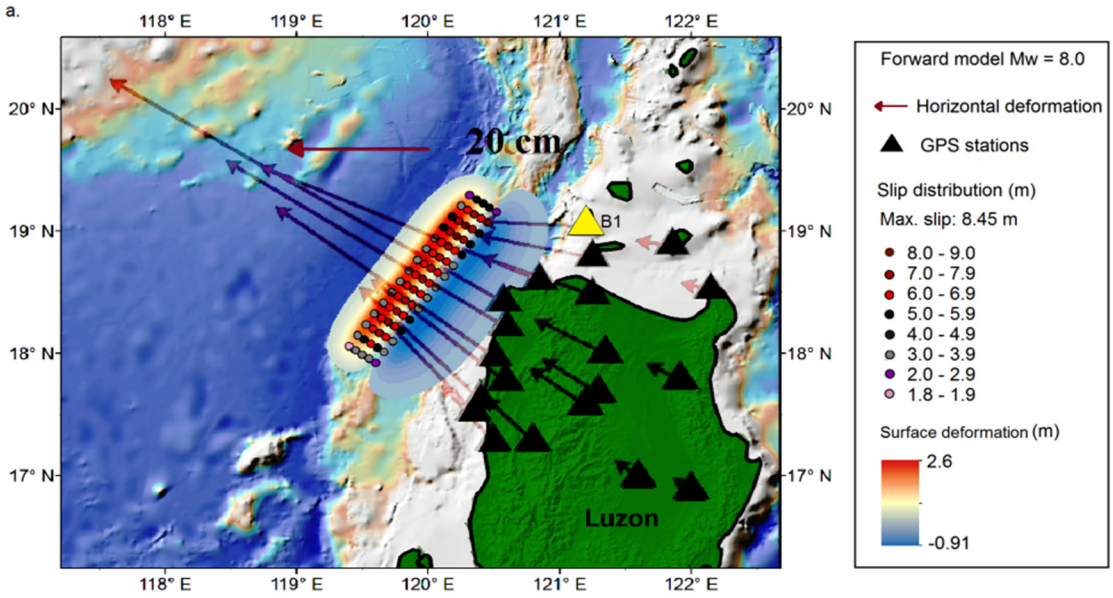

Figure 4. *Cont.*

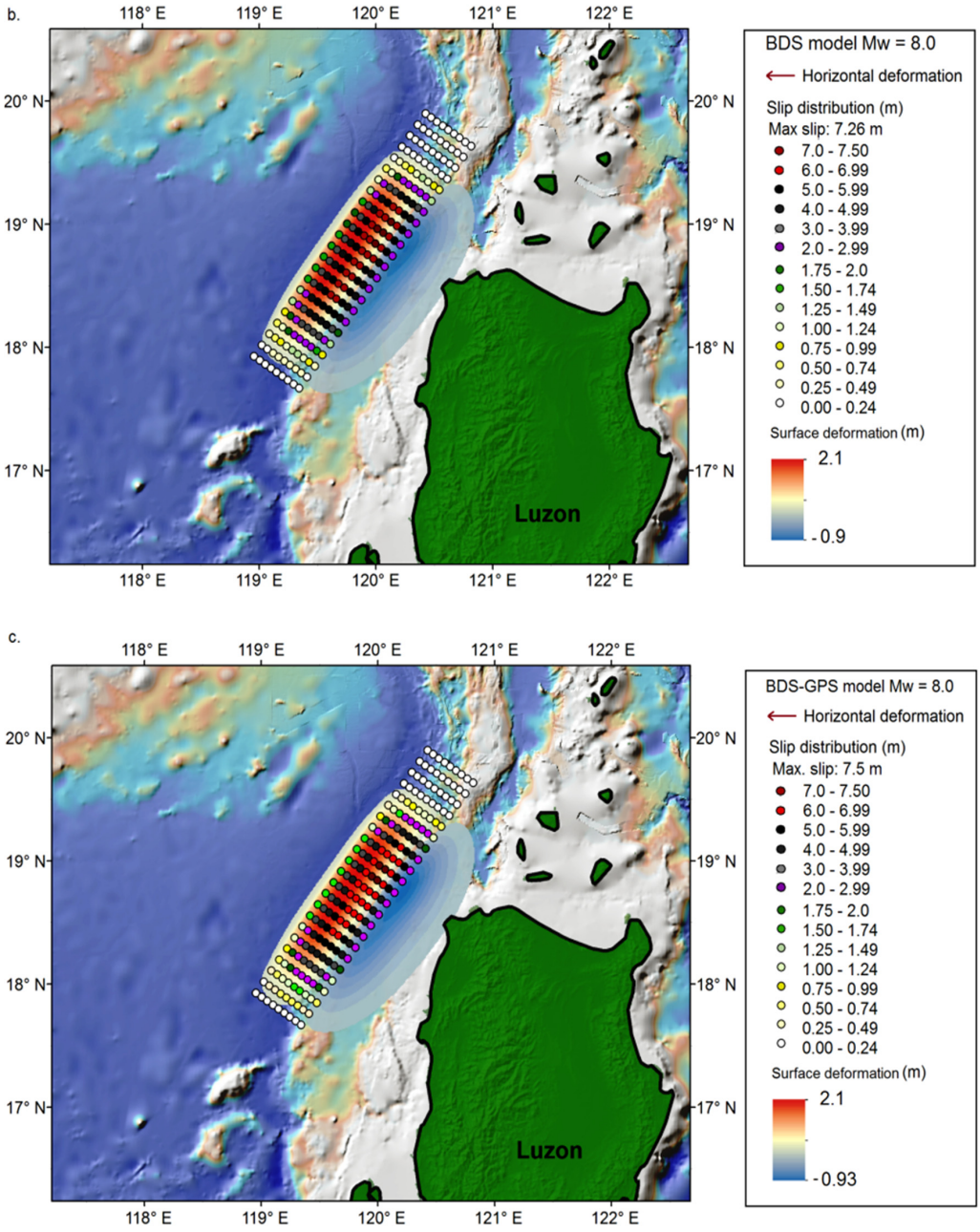

Figure 4. (**a**) Assumed slip distribution (colored dots) and correspondent co-seismic surface deformation for an event with a magnitude of Mw = 8.0 rupturing along the Northern Manila mega-thrust: our forward-model scenario. Red arrows show horizontal displacements computed at the virtual BDS/GPS network (black triangles). The yellow triangle (B1) marks the station from Figure 3; (**b**) Colored dots represent slip distribution as inverted from the simulated BDS-displacements (note, synthetic BDS-displacements include real-time processing noise). Additionally shown is the resulting vertical deformation; (**c**) Same as (**b**), but for the inversion of the joint BDS/GPS displacements.

Based on the suggested rupture, the corresponding tsunami scenario was simulated (Figure 5) using the *easyWave* wave propagation code [20]. *easyWave* follows the numerical algorithm by Goto *et al.* [44] for the simulation of linear long-wave propagation in spherical coordinates. Tsunami propagation was computed on the 1 arc minute GEBCO (General Bathymetric Chart of the Oceans) bathymetric grid [45], and the sea-level heights at offshore positions were projected to the

coast using Green's amplification law [46]. As expected, due to the predominantly SW-NE orientation of the rupture, main tsunami energy is radiated towards the southeastern coast of China, between the cities of Hong Kong and Shantou (Figure 5). Expected maximum tsunami wave heights may reach up to 10 m at the west coast of the Luzon Island. At the southwest coast of Taiwan and southeastern coast of China, tsunami wave heights may reach 1–2 m.

In order to issue a reliable tsunami early warning as soon as possible, seismic parameters (e.g., epicenter, magnitude, slip distribution) should be inverted from co-seismic signal immediately after the earthquake breaks. Since the Luzon Island is located close to the northern Manila trench, our scenario rupture causes significant horizontal co-seismic displacements throughout the island. As shown in Figure 4a, stations distributed along the northwest part of the Luzon Island will experience northwest-directed surface displacements in excess of 10 cm. Taking into account the horizontal accuracy of real-time BDS and GPS processing of about 1 cm (Table 1), we conclude that co-seismic displacements due to an earthquake with a size of Mw = 8.0 should be well-detected and accurately measured with the present-day BDS/GPS observation and processing precision, which, in turn, should enable reliable source inversion and tsunami forecasting.

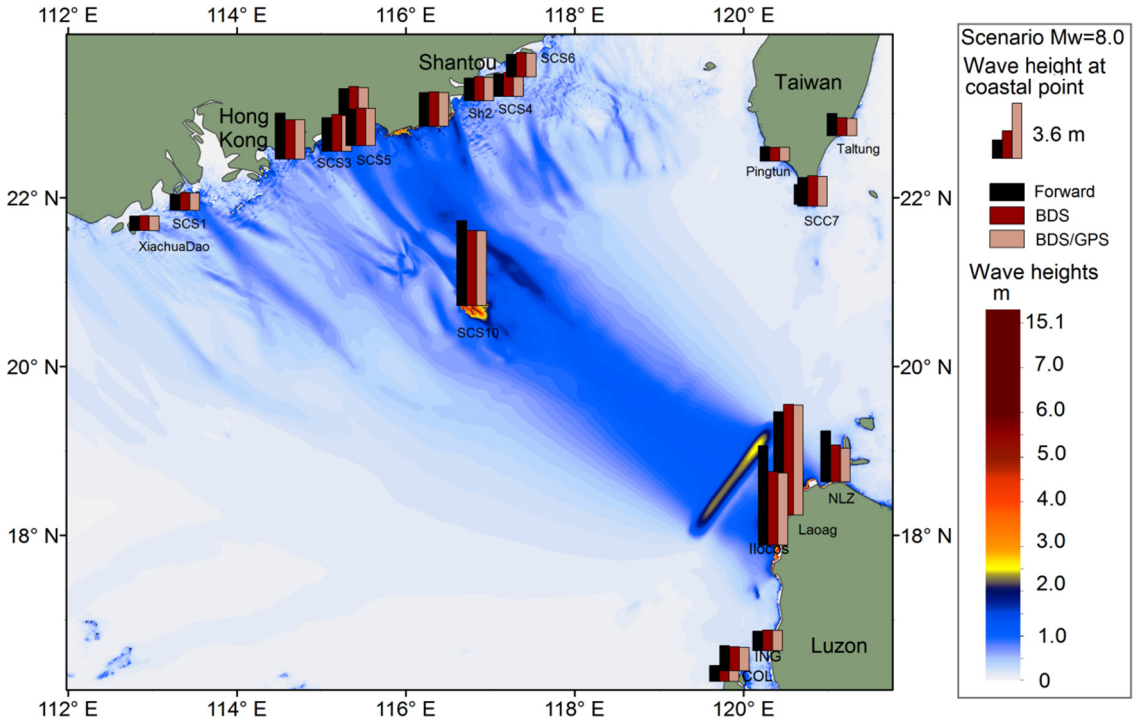

Figure 5. Simulated tsunami scenarios. The color map shows the maximum wave height in the forward model (Figure 4a) after 6 h of tsunami propagation. Vertical bars are maximum wave heights as recorded at selected coastal locations for the three propagation models: forward model (black); with source as inverted from BDS-displacements (dark grey in Figure 4b); with source as inverted from joint BDS/GPS-displacements (light grey, Figure 4c).

To illustrate this, we retrieved static offsets from our simulated kinematic BDS and BDS/GPS displacements (Figure 3) and invert them back into the source parameters (Figure 4b,c). Finally, we compute tsunami propagations from the "inverted sources" and compare them to the forward scenario (vertical bars on Figure 5). In order to get static offsets at virtual BDS/GPS stations from the contaminated displacement waveforms (Figure 3), we employ a method introduced by Ohta *et al.* [21]. Resulting static displacements were subsequently inverted into the slip distribution along the predefined geometry of the Manila trench using the SDM software [47]. Here, in order to make the inversion test closer to the real world scenario, we did not constrain the possible rupture

geometry to the forward model area by length and width. Additionally, we employed alternative fault discretization with 23 × 9 subfaults. Since we were expecting predominantly thrust events at the Manila trench, the rake angle was allowed to vary between 70 and 100 degrees. The two horizontal components were weighted twice as much as the vertical component, and a smoothing constraint was imposed to avoid unrealistic slip patterns.

Figure 4b,c present slip distributions as inverted from the simulated real-time co-seismic BDS (Figure 4b) and joint BDS/GPS (Figure 4c) displacements. Inverted slip distributions from single BDS and BDS/GPS show a high degree of consistency, which is obvious since the processing accuracy is very similar in both cases (Table 1). In contrast, comparison with the forward model (Figure 4a) shows some bias. To be exact, inverted slip distribution covers a somewhat larger area than the original model; the maximum slip of the forward model is 8.4 m while the inverted maximum slips are 7.31 and 7.32 m, respectively, and the derived moment magnitudes are both Mw = 8.06, slightly greater than the input value of Mw = 8.0. This insignificant discrepancy is explained, first of all, by the fact that our virtual observational network is located, due to natural reasons, only on one side of the Manila trench. Nevertheless, tsunami wave heights as predicted from the inverted source models are very similar to the forward computations (compare vertical bars on Figure 5 and refer to the supplementary Table S1 for more detailed information). Note that the difference in estimated wave heights is larger along the Luzon coast compared to the distant coasts of China and Taiwan. This demonstrates the known fact that, for reliable near-field tsunami early warnings, a trustworthy slip distribution is favorable.

From this synthetic inversion test, we conclude that a BDS (or a BDS/GPS) network with real-time processing, if deployed at the Luzon Island, will be able to contribute to a fast and reliable tsunami source inversion at the Manila trench.

4. Discussions

As we have noted before, precise real-time GNSS processing is a prerequisite for incorporation of coastal GNSS-arrays into tsunami early warnings. In this context, we assessed the potential capability of using real-time BDS to detect on-land co-seismic displacements caused by submarine rupture and addressed the special contribution from combined BDS/GPS solutions as well. According to our estimations from Section 2, horizontal accuracies of single BDS and GPS at the test site were 1.1 cm and 1.2 cm, respectively, while the joint BDS/GPS accuracy reached about 0.7 cm. For vertical component, BDS/GPS improved accuracy from about 2 cm to about 1.0 cm. In terms of current accuracy, BDS is close to GPS in the Asia-Pacific region, and the advantage of fusion of BDS and GPS is clear. Nonetheless, our simulation of the Mw = 8.0 earthquake did not show any notable difference in the case of BDS-only or BDS/GPS joint inversion (compare Figure 4b,c). For an earthquake with a magnitude of Mw = 8.0, near field deformation can be as large as tens of centimeters (Figure 4a); with respect to this scale of deformation, the signal-to-noise ratio (SNR) improvement by joint BDS/GPS processing is not clear in this case. However, joint BDS/GPS processing may show its advantage for smaller but still tsunamigenic earthquakes.

Consider a scenario of a smaller earthquake. Figure 6 presents a forward model as well as the two source inversion models for an Mw = 7.5 earthquake at the Manila trench (compare Figure 6 to Figure 4). Earthquakes of this magnitude will not pose a significant tsunami threat for the coasts of China and Taiwan but can still be dangerous in the near field (Figure 7). In this case, simulated co-seismic displacements are significantly smaller (Figure 6a), and the better signal-to-noise ratio of the joint BDS/GPS real-time processing results in better restoration of the original slip distribution (compare Figure 6b,c) and, therefore, in better tsunami forecasting for the near field (compare vertical bars on Figure 7 and refer to the supplementary Table S1 for more detailed information).

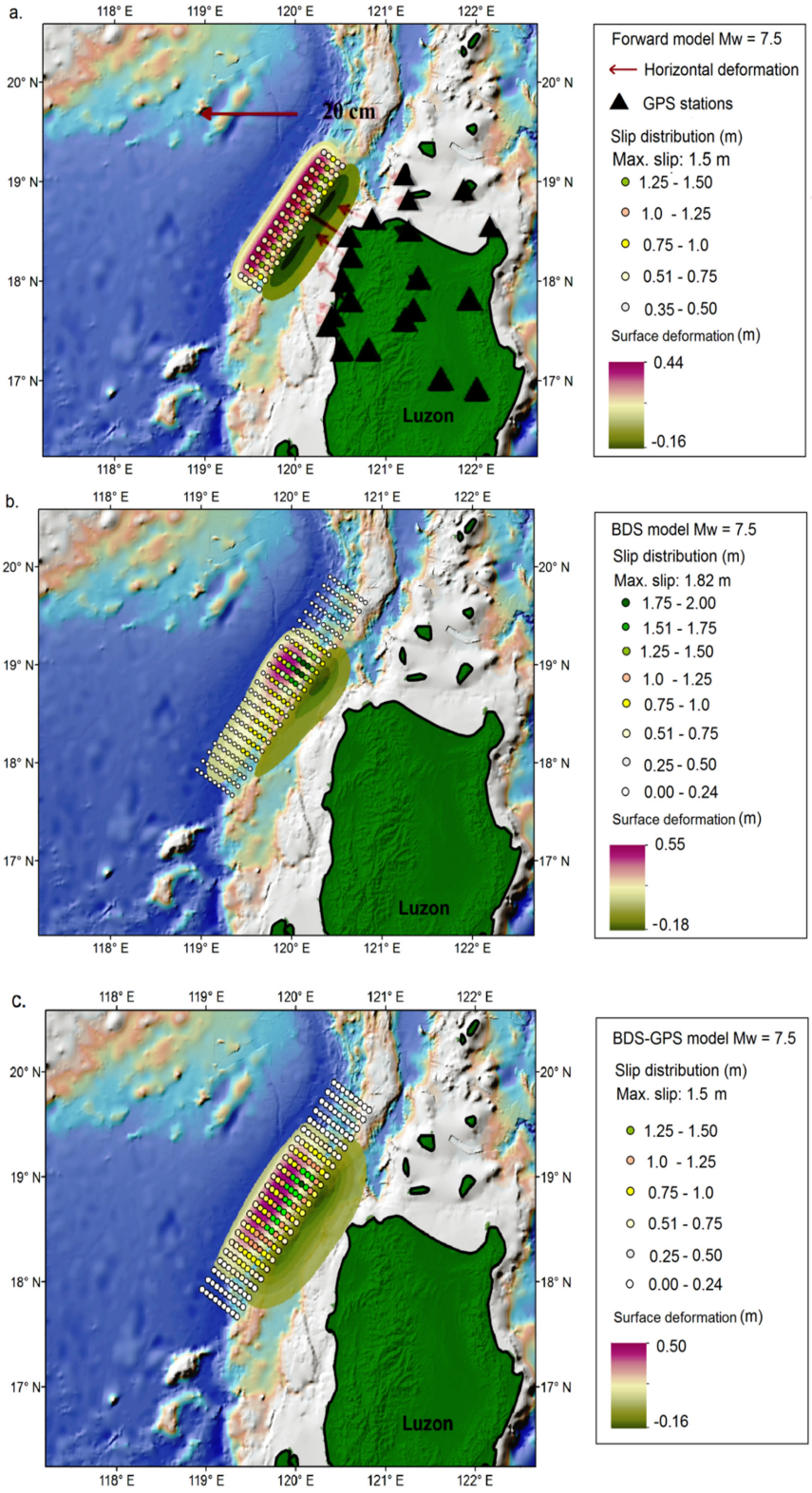

Figure 6. (**a**) Assumed slip distribution (colored dots) and correspondent co-seismic surface deformation for an event with a magnitude of Mw = 7.5 rupturing along the Northern Manila mega-thrust. Red arrows show horizontal displacements computed at the virtual BDS/GPS network (black triangles); (**b**) Colored dots show slip distribution as inverted from the simulated BDS-displacements (note, synthetic BDS-displacements include real-time processing noise). Additionally shown is the resulting vertical deformation; (**c**) Same as (b), but for the inversion of the joint BDS/GPS displacements.

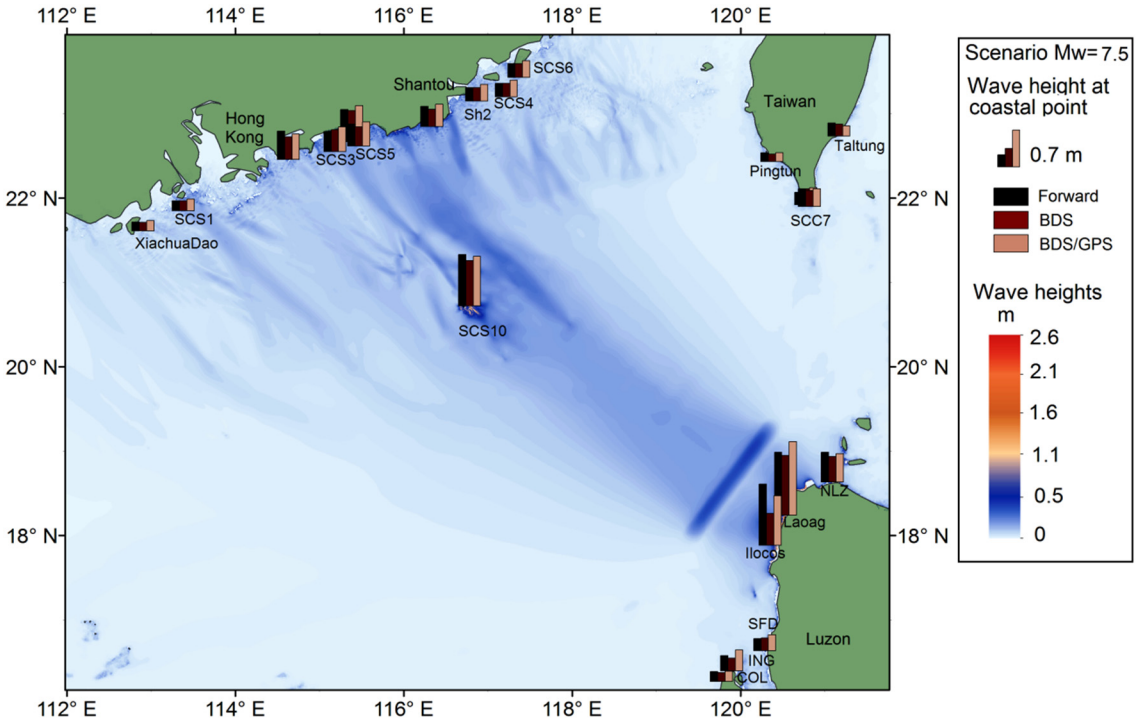

Figure 7. Simulated tsunami scenarios. The color map shows the maximum wave height in the forward model (Figure 6a) after 6 h of tsunami propagation. Vertical bars are maximum wave heights as recorded at selected coastal locations for the three propagation models: the forward model (black); the model with the source as inverted from BDS-displacements (dark grey, Figure 6b); and the model with the source as inverted from joint BDS/GPS-displacements (light grey, Figure 6c).

Notice that our models are simple and generic enough to illustrate the main message of the present study: Tsunamigenic earthquakes at the Manila trench will trigger significant co-seismic deformation at the Luzon Island. Deformation amplitudes will be far above modern real-time GNSS resolution. That is why it makes sense to employ coastal GNSS-arrays for tsunami early warnings in the Southern China Sea.

At the same time, authors understand that there are many open questions regarding practical incorporation of GNSS component into any particular TEWS. For example, we opted for static inversion of final co-seismic displacements. Alternatively, some very recent studies [48,49] showed that static inversions have a tendency to over-smoothen slip distribution, which, in turn, can result in the under-prediction of tsunami heights. Kinematic (waveform) inversions demonstrate better spatial resolution and have a clear advantage when static displacements are small. On the other hand, static inversions are fast and robust, and use less data and a smaller number of control parameters.

The problem of optimal choice of methods and algorithms is not, of course, restricted to static *vs.* kinematic inversion. If the source alone is considered—the GNSS array distribution; the source forward model, which includes geometry, the elastic model, slip distribution; inversion algorithm itself—there is only a short list of issues requiring testing and optimization. It is the same for tsunami simulation and decision-making; each of them also have dozens of options. Authors believe that decisions about better methods and better practices should be taken on an individual basis, in harmonization within particular TEWS and its individual components.

5. Conclusions

In this study, we investigated the precise positioning performance of BDS and BDS/GPS in the Asia-Pacific region, and we specifically focused on their applications to tsunami early warnings

in the SCS region. By analyzing two MGEX stationary stations, we demonstrated that BDS and GPS display similar positioning accuracy in the Asia-Pacific region. Combined BDS/GPS solution not only shows a somewhat higher degree of precision but, what is even more important for operational implementation in decision-making applications like tsunami early warnings, also improves the robustness.

By considering a scenario of a devastating tsunami in the Southern China Sea triggered by a Mw = 8.0 earthquake along the Manila trench, we propose deploying a continuous BDS/GPS-network at the western coast of the Luzon Island, Philippines. This network, if complemented with the modern real-time processing technique (here TPP), will contribute to a very fast (2–3 min) earthquake evaluation and source inversion, moving toward a higher reliability of the local and regional tsunami early warning.

Using a scenario with a smaller but still tsunamigenic earthquake (Mw = 7.5), we demonstrate that the advantage of combined BDS/GPS over single GNSS processing by source inversion grows with decreasing earthquake magnitudes. To conclude, BDS and BDS/GPS can become an important component of the future TEWS in the SCS, although numerous factors need to be optimized in future studies.

Considering that the BDS constellation is still under construction, with increasing numbers of BDS satellites and ground-tracking stations arising in the coming years, its visibility in other places in the world will improve significantly, and the orbit and clock bias products will be more accurate, which indicate that precision of BDS is expected to be equal on a global level. That is to say, the concept of BDS and BDS/GPS as a tsunami early warning component is not limited to the Asia-Pacific region, but will be able to be applied worldwide.

Acknowledgments: K.C. is supported by the China Scholarship Council (CSC) for his PhD study in the German Research Centre for Geoscience. N.Z. is supported by the Helmholtz Association through the GeoSim program. This study was also supported by the National Natural Science Foundation of China (Grant No. 41504010; 41574027; 41325015; 41231174). We appreciate valuable comments from the three reviewers which improve this manuscript greatly.

Author Contributions: Kejie Chen initialized the idea and conception; Kejie Chen, Natalia Zamora and Andrey Babeyko wrote the manuscript; All authors reviewed the manuscript.

Conflicts of Interest: The authors declare no conflict of interest.

References

1. NGDC/WDS National Geophysical Data Center/World Data Service (NGDC/WDS). Available online: http://www.ngdc.noaa.gov/hazard/tsu_db.shtml (accessed on 23 November 2015).
2. Japan Meteorological Agency (JMA). *Lessons Learned from the Tsunami Disaster Caused by the 2011 Great East Japan Earthquake and Improvements in JMA' s Tsunami Warning System*; Japan Meteorological Agency: Tokyo, Japan, 2013.
3. Boore, D.M.; Bommer, J.J. Processing of strong-motion accelerograms: Needs, options and consequences. *Soil Dyn. Earthq. Eng.* **2005**, *25*, 93–115. [CrossRef]
4. Melgar, D.; Bock, Y.; Sanchez, D.; Crowell, B.W. On robust and reliable automated baseline corrections for strong motion seismology. *J. Geophys. Res. Solid Earth* **2013**, *118*, 1177–1187. [CrossRef]
5. Hirose, F.; Miyaoka, K.; Hayashimoto, N.; Yamazaki, T.; Nakamura, M. Outline of the 2011 off the Pacific coast of Tohoku Earthquake (Mw 9.0)—Seismicity: Foreshocks, mainshock, aftershocks, and induced activity. *Earth Planets Space* **2011**, *63*, 513–518. [CrossRef]
6. Bormann, P.; Saul, J. A fast, non-saturating magnitude estimator for great earthquakes. *Seismol. Res. Lett.* **2009**, *80*, 808–816. [CrossRef]
7. Hanka, W.; Saul, J.; Weber, B.; Becker, J.; Harjadi, P. Real-time earthquake monitoring for tsunami warning in the Indian Ocean and beyond. *Nat. Hazards Earth Syst. Sci.* **2010**, *10*, 2611–2611. [CrossRef]
8. Kanamori, H.; Rivera, L. Source inversion of W phase: Speeding up seismic tsunami warning. *Geophys. J. Int.* **2008**, *175*, 222–238. [CrossRef]

9. Duputel, Z.; Rivera, L.; Kanamori, H.; Hayes, G.P.; Hirshorn, B.; Weinstein, S. Real-time W phase inversion during the 2011 off the Pacific coast of Tohoku Earthquake. *Earth Planets Space* **2011**, *63*, 535–539. [CrossRef]
10. Lomax, A.; Michelini, A. Mwpd: A duration-amplitude procedure for rapid determination of earthquake magnitude and tsunamigenic potential from P waveforms. *Geophys. J. Int.* **2009**, *176*, 200–214. [CrossRef]
11. Wang, R.; Schurr, B.; Milkereit, C.; Shao, Z.; Jin, M. An improved automatic scheme for empirical baseline correction of digital strong-motion records. *Bull. Seismol. Soc. Am.* **2011**, *101*, 2029–2044. [CrossRef]
12. Tu, R.; Wang, R.; Zhang, Y.; Walter, T.R. Application of a net-based baseline correction scheme to strong-motion records of the 2011 Mw 9.0 Tohoku earthquake. *Geophys. J. Int.* **2014**, *204*. [CrossRef]
13. Bock, Y.; Melgar, D.; Crowell, B.W. Real-time strong-motion broadband displacements from collocated GPS and accelerometers. *Bull. Seismol. Soc. Am.* **2011**, *101*, 2904–2925. [CrossRef]
14. Li, X.; Ge, M.; Zhang, Y.; Wang, R.; Guo, B.; Klotz, J.; Wickert, J.; Schuh, H. High-rate coseismic displacements from tightly integrated processing of raw GPS and accelerometer data. *Geophys. J. Int.* **2013**, *195*. [CrossRef]
15. Crowell, B.W.; Melgar, D.; Bock, Y.; Haase, J.S.; Geng, J. Earthquake magnitude scaling using seismogeodetic data. *Geophys. Res. Lett.* **2013**, *40*, 6089–6094. [CrossRef]
16. Blewitt, G.; Kreemer, C.; Hammond, W.C.; Plag, H.-P.; Stein, S.; Okal, E. Rapid determination of earthquake magnitude using GPS for tsunami warning systems. *Geophys. Res. Lett.* **2006**, *33*, L11309–L11309. [CrossRef]
17. Sobolev, S.V.; Babeyko, A.Y.; Wang, R.; Hoechner, A.; Galas, R.; Rothacher, M.; Sein, D.V.; Schröter, J.; Lauterjung, J.; Subarya, C. Tsunami early warning using GPS-Shield arrays. *J. Geophys. Res. Solid Earth* **2007**, *112*, B08415. [CrossRef]
18. Babeyko, A.Y.; Hoechner, A.; Sobolev, S.V. Source modeling and inversion with near real-time GPS: A GITEWS perspective for Indonesia. *Nat. Hazards Earth Syst. Sci.* **2010**, *10*, 1617–1627. [CrossRef]
19. Falck, C.; Ramatschi, M.; Subarya, C.; Bartsch, M.; Merx, A.; Hoeberechts, J.; Schmidt, G. Near real-time GPS applications for tsunami early warning systems. *Nat. Hazards Earth Syst. Sci.* **2010**, *10*, 181–189. [CrossRef]
20. Hoechner, A.; Ge, M.; Babeyko, A.Y.; Sobolev, S.V. Instant tsunami early warning based on real-time GPS—Tohoku 2011 case study. *Nat. Hazards Earth Syst. Sci.* **2013**, *13*, 1285–1292. [CrossRef]
21. Ohta, Y.; Kobayashi, T.; Tsushima, H.; Miura, S.; Hino, R.; Takasu, T.; Fujimoto, H.; Iinuma, T.; Tachibana, K.; Demachi, T.; *et al*. Quasi real-time fault model estimation for near-field tsunami forecasting based on RTK-GPS analysis: Application to the 2011 Tohoku-Oki earthquake (Mw 9.0). *J. Geophys. Res. Solid Earth* **2012**, *117*. [CrossRef]
22. Wright, T.J.; Houlié, N.; Hildyard, M.; Iwabuchi, T. Real-time, reliable magnitudes for large earthquakes from 1 Hz GPS precise point positioning: The 2011 Tohoku-Oki (Japan) earthquake. *Geophys. Res. Lett.* **2012**. [CrossRef]
23. Melgar, D.; Bock, Y.; Crowell, B.W. Real-time centroid moment tensor determination for large earthquakes from local and regional displacement records. *Geophys. J. Int.* **2012**, *188*, 703–718. [CrossRef]
24. Melgar, D.; Crowell, B.W.; Geng, J.; Allen, R.M.; Bock, Y.; Riquelme, S.; Hill, E.M.; Protti, M.; Ganas, A. Earthquake magnitude calculation without saturation from the scaling of peak ground displacement. *Geophys. Res. Lett.* **2015**, *42*, 5197–5205. [CrossRef]
25. Li, X.; Ge, M.; Zhang, X.; Zhang, Y.; Guo, B.; Wang, R.; Klotz, J.; Wickert, J. Real-time high-rate co-seismic displacement from ambiguity-fixed precise point positioning: Application to earthquake early warning. *Geophys. Res. Lett.* **2013**, *40*, 295–300. [CrossRef]
26. Fang, R.; Shi, C.; Song, W.; Wang, G.; Liu, J. Determination of earthquake magnitude using GPS displacement waveforms from real-time precise point positioning. *Geophys. J. Int.* **2013**, *196*, 461–472. [CrossRef]
27. Zhao, Q.; Guo, J.; Li, M.; Qu, L.; Hu, Z.; Shi, C.; Liu, J. Initial results of precise orbit and clock determination for COMPASS navigation satellite system. *J. Geod.* **2013**, *87*, 475–486. [CrossRef]
28. Li, M.; Qu, L.; Zhao, Q.; Guo, J.; Su, X.; Li, X. Precise Point Positioning with the BeiDou Navigation Satellite System. *Sensors* **2014**, *14*, 927–943. [CrossRef] [PubMed]
29. Li, X.; Ge, M.; Dai, X.; Ren, X.; Fritsche, M.; Wickert, J.; Schuh, H. Accuracy and reliability of multi-GNSS real-time precise positioning: GPS, GLONASS, BeiDou, and Galileo. *J. Geod.* **2015**, *89*, 607–635. [CrossRef]
30. Liu, P.L.-F.; Wang, X.; Salisbury, A.J. Tsunami hazard and early warning system in South China Sea. *J. Asian Earth Sci.* **2009**, *36*, 2–12. [CrossRef]

31. Dao, M.H.; Tkalich, P.; Chan, E.S.; Megawati, K. Tsunami propagation scenarios in the South China Sea. *J. Asian Earth Sci.* **2009**, *36*, 67–73. [CrossRef]
32. Okal, E.A.; Synolakis, C.E.; Kalligeris, N. Tsunami simulations for regional sources in the South China and adjoining seas. *Pure Appl. Geophys.* **2010**, *168*, 1153–1173. [CrossRef]
33. Suppasri, A.; Imamura, F.; Koshimura, S. Tsunami hazard and casualty estimation in a coastal area the neighbors the Indian Ocean and South China Sea. *J. Earthq. Tsunami* **2012**, *6*, 1250010. [CrossRef]
34. Sun, L.; Zhou, X.; Huang, W.; Liu, X.; Yan, H.; Xie, Z.; Wu, Z.; Zhao, S.; Shao, D.; Yang, W. Preliminary evidence for a 1000-year-old tsunami in the South China Sea. *Sci. Rep.* **2013**, *3*. [CrossRef] [PubMed]
35. Lau, A.Y.A.; Switzer, A.D.; Dominey-Howes, D.; Aitchison, J.C.; Zong, Y. Written records of historical tsunamis in the northeastern South China Sea—Challenges associated with developing a new integrated database. *Nat. Hazards Earth Syst. Sci.* **2010**, *10*, 1793–1806. [CrossRef]
36. Jing, H.; Zhang, H.; Yuen, D.; Shi, Y. A revised evaluation of tsunami hazards along the Chinese coast in view of the Tohoku-Oki Earthquake. *Pure Appl. Geophys.* **2013**, *170*, 129–138. [CrossRef]
37. Ren, Z.-Y.; Liu, H.; Wang, B.-L.; Zhao, X. An investigation on multi-buoy inversion method for Tsunami Warning System in South China Sea. *J. Earthq. Tsunami* **2014**, *8*. [CrossRef]
38. An, C. Inversion of Tsunami Waveforms and Tsunami warning. Ph.D. Thesis, The Cornell University, Ithaca, NY, USA, June 2015.
39. Colosimo, G.; Crespi, M.; Mazzoni, A. Real-time GPS seismology with a stand-alone receiver: A preliminary feasibility demonstration. *J. Geophys. Res. Solid Earth* **2011**, *116*. [CrossRef]
40. Li, X.; Ge, M.; Guo, B.; Wickert, J.; Schuh, H. Temporal point positioning approach for real-time GNSS seismology using a single receiver. *Geophys. Res. Lett.* **2013**, *40*, 5677–5682. [CrossRef]
41. Kirby, S.; Geist, E. Great earthquake tsunami sources: Empiricism and beyond. In Proceedings of the USGS Tsunami Sources Workshop, Menlo Park, CA, USA, 21–22 April 2006.
42. Wang, R. Tidal response of the solid Earth. In *Tidal Phenomena*; Springer: Heidelberg, Germany, 1997; pp. 27–57.
43. Kennett, B.L.N.; Engdahl, E.R.; Buland, R. Constraints on seismic velocities in the Earth from traveltimes. *Geophys. J. Int.* **1995**, *122*, 108–124. [CrossRef]
44. Goto, C.; Ogawa, Y.; Shuto, N.; Imamura, F. *IUGG/IOC Time Project, Numerical Method of Tsunami Simulation with the Leap-Frog Scheme*; IOC Manuals and Guides No. 35; Unesco: Paris, Frace, 1997.
45. Smith, W.H.F.; Sandwell, D. Global sea floor topography from satellite altimetry and ship depth soundings. *Science* **1997**, *277*, 1956–1962. [CrossRef]
46. Kamigaichi, O. Tsunami Forecasting and Warning. In *Encyclopedia of Complexity and Systems Science SE—568*; Meyers, R.A., Ed.; Springer: New York, NY, USA, 2009; pp. 9592–9618.
47. Wang, L.; Wang, R.; Roth, F.; Enescu, B.; Hainzl, S.; Ergintav, S. Afterslip and viscoelastic relaxation following the 1999 M 7.4 İzmit earthquake from GPS measurements. *Geophys. J. Int.* **2009**, *178*, 1220–1237. [CrossRef]
48. Melgar, D.; Bock, Y. Near-field tsunami models with rapid earthquake source inversions from land- and ocean-based observations: The potential for forecast and warning. *J. Geophys. Res. Solid Earth* **2013**, *118*, 5939–5955. [CrossRef]
49. Melgar, D.; Bock, Y. Kinematic earthquake source inversion and tsunami runup prediction with regional geophysical data. *J. Geophys. Res. Solid Earth* **2015**, *120*, 3324–3349. [CrossRef]